Evidence for chiral symmetry breaking in ^{140}Eu?

A. A. Hecht,[1,*] C. W. Beausang,[1] H. Amro,[1] C. J. Barton,[1,2,†] Z. Berant,[1,2,3] M. A. Caprio,[1] R. F. Casten,[1] J. R. Cooper,[1,‡] D. J. Hartley,[4,§] R. Krücken,[4,‖] D. A. Meyer,[1] H. Newman,[1] J. R. Novak,[1] N. Pietralla,[1,5,¶] J. J. Ressler,[1] A. Wolf,[1,2,3] N. V. Zamfir,[1,6] Jing-Ye Zhang,[4] and K. E. Zyromski[1]

[1] *Yale University, New Haven, Connecticut 06520, USA*

[2] *Department of Physics, Clark University, Worcester, Massachusetts 10610, USA*

[3] *Nuclear Research Center-Negev, Beer Sheva 84190, Israel*

[4] *Department of Physics and Astronomy, University of Tennessee, Knoxville, Tennessee 37996, USA*

[5] *Department of Physics and Astronomy, SUNY at Stony Brook, Stony Brook, New York 11794, USA*

[6] *National Institute for Physics and Nuclear Engineering, Bucharest, Romania*

(Received 25 July 2003; published 21 November 2003)

High spin states in ^{140}Eu were populated following the reaction ^{92}Mo(^{51}V, $2pn$) at a beam energy of 205 MeV by the ESTU accelerator at the Wright Nuclear Structure Laboratory, Yale University. A total of 5 bands and 69 transitions were assigned to ^{140}Eu. The assignments were based on K_α x-ray coincidences and on excitation function measurements. γ-γ and γ-γ-γ coincidence matrices were created. Directional correlation of oriented states analysis, angular distributions, and Compton asymmetry measurements were performed and $B(M1)/B(E2)$ branching ratios were extracted. The band assignments and structures are discussed in terms of the rotational model and interpreted following a series of cranked shell model and total Routhian surface calculations. In particular, two pairs of bands, one pair based on the $\pi h_{11/2} \otimes \nu h_{11/2}$ configuration, the other based on the $\pi(g_{7/2}, d_{5/2}) \otimes \nu h_{11/2}$ configuration, are identified. These bands show some features expected of either chiral partners or shape coexistence, based on triaxial shapes with $\gamma \sim \pm 25°$. Further measurements are required to distinguish between these two possibilities.

DOI: 10.1103/PhysRevC.68.054310 PACS number(s): 21.10.Re, 23.20.Lv, 27.60.+j, 23.90.+w

I. INTRODUCTION

The moderately deformed ($\beta \sim 0.2$) nuclei in the mass $A \sim 130$ region with $Z \sim 60$–65 and $N \sim 75$ have long been considered to be γ soft [1], the degree of γ deformation depending on the polarizing influence of the valence quasiparticles [2]. The γ softness and shape polarization make this region particularly interesting for shape driven effects. Coexistence of different shapes is one well known effect in this region [3], in which several different deformations of the nucleus may exist at nearly the same excitation energy and spin. In addition, in triaxially deformed odd-odd nuclei, the suggestion that these nuclei may exhibit a type of dynamic chiral symmetry [4] has sparked a flurry of experimental activity and renewed interest in the study of the intermediate spin structure of such nuclei. Indeed, chiral twin band candidates have been reported in several nuclei with $N \sim 75$ and Z ranging from 57 to 63 [5]. Briefly, the idea of Ref. [4] is the following. A deformed nucleus with a finite γ deformation possesses three distinct principal axes, the short, intermediate, and long axes, which together define a coordinate system in the nuclear frame. For doubly odd nuclei and for a suitable choice of particle number, the unpaired single particle angular momentum vectors j_π (protons) and j_ν (neutrons) may tend to align along the short and long axes, respectively. This is the case in the mass $A \sim 130$ region where the proton Fermi surface is low, and the neutron Fermi surface high in the high-j $h_{11/2}$ shell. In addition, since the moment of inertia for rotation about the intermediate nuclear axis is the largest, due to irrotational flow [6], the collective rotational angular momentum vector R will tend to align along this axis. Thus, schematically, for intermediate spins where the magnitude of R is comparable to j_π and j_ν, the total angular momentum lies not only off of any principal axis but out of any principal plane. The orientation of this total angular momentum vector with respect to the nuclear axes defines two distinct coordinate systems, differing only in their handedness or chirality. In this case, aplanar tilted axis cranking model calculations [4] predict a doubling of states and the occurrence of two pairs of degenerate $\Delta I = 1$ bands of the same orbital configuration and parity, with levels of the same spin being degenerate. However, the energy degeneracy should persist only over a limited range of spins, roughly speaking, only for those spin values where the total angular momentum vector points significantly out of the principal planes, i.e., where R is roughly comparable to j_π and j_ν. For a finite barrier between the two chiral solutions, mixing is possible which will break the energy degeneracy of these bands. Thus, the experimental manifestation of this effect is expected to be two pairs of $\Delta I = 1$ bands with the same spins, parities, orbital assignments, and branching ratios, with similar transition en-

*Electronic address: adam.hecht@yale.edu

†Present address: CLRC Daresbury Laboratory, UK.

‡Present address: Lawrence Livermore National Laboratory, Livermore, CA 94551, USA.

§Present address: Department of Physics, U.S. Naval Academy, Annapolis, MD 21402, USA.

‖Permanent address: Physik Department E12, Technische Universität München, 85748 Garching, Germany.

¶Present address: Universität zu Köln, Köln, Germany.

ergies, possibly offset from each other. This energy splitting is distinct from signature splitting, and in most chiral band candidates in the region, the splitting is several hundred keV less than predictions for signature splitting [7], which is less by a factor of 2 or so. Note that for tilted axis cranking [8] signature is not a good quantum number but the term is used in this work for ease of comparison with the better known principal axis cranking model [9], in which the total angular momentum is aligned along a principal axis of the nucleus.

Recently, several doubly odd nuclei in the mass $A\sim130$ [5], $A\sim110$ [10], and $A\sim190$ [11] regions have been shown to possess such chiral partner bands. Most examples have been found in the $N=75$ isotones, from ^{130}Cs to ^{138}Eu, with several other cases in the neighboring $N=73$ (Cs-Pr) and $N=77$ (Cs-La) isotones. In all the cases in the odd-odd $A\sim130$ nuclei, the bands are based on the $\pi h_{11/2}\otimes\nu h_{11/2}$ microscopic configuration. The doubly-odd ^{140}Eu ($N=77, Z=63$) nucleus lies at the extremes of both the N and Z ranges in which chiral structures have been found in this mass region. It is at the limit where the proton and neutron Fermi surfaces are optimal for the required perpendicular coupling of the single particle angular momenta (for example, for $Z=63$ and $N=77$ the $\Omega=3/2$ proton and 11/2 neutron projections of the $h_{11/2}$ orbitals are lowest). Clearly it is of great interest to probe this nucleus, to test the limits of this region of chiral symmetry.

For essentially any low lying configuration, total Routhian surface (TRS) calculations [12] for ^{140}Eu show well developed potential energy minima that are close in energy near both $\gamma=+25°$ and $-25°$ which persist up to high frequencies. These two minima at $\beta\sim0.2$ and $\gamma=\pm25°$ open up the possibility of another interesting phenomenon in ^{140}Eu, namely, shape coexistence. Indeed, shape coexistence is well known in several nuclei in the region [3], typically occurring for bands based on different orbital configurations which polarize the core to different shapes. However, in the even-even core of ^{140}Eu(^{138}Sm), two bands having the same orbital configuration [13] but different deformations are observed. In that example, for one deformation the band built on the $\pi(h_{11/2},g_{7/2})\otimes\nu(h_{11/2})^2$ configuration shows a negligible signature splitting. For the other band built on the same orbital configuration, only one signature is observed.

Until recently, the low spin states in ^{140}Eu were known from β decay, up to a 125 ms, 5^- isomeric level at an excitation energy of <234 keV, given in Ref. [14]. Recently, other independent studies of ^{140}Eu were carried out [15–17]. Several bands have been reported based on prompt coincidence data [15]. The isomer decay tagging method was used to identify several transitions which feed the 5^- level as well as a new, higher lying, $\sim$300 ns isomer [16]. Two rotational bands were reported, assigned as the $\pi h_{11/2}\otimes\nu h_{11/2}$ and $\pi h_{11/2}\otimes\nu g_{7/2}$ configurations, feeding into the $\sim$300 ns and into the 125 ms, 5^-, isomeric levels, respectively [17].

In the current work, high statistics γ triples prompt coincidence data were used to develop and greatly expand the level scheme for ^{140}Eu. Transitions were identified with ^{140}Eu based on K_α coincidence and through an excitation function. Other transitions were identified as belonging to ^{140}Eu through coincidence analysis involving the directly identified transitions. While confirming several of the results reported in Refs. [15–17], we also report many new levels and several new bands. Several of the transitions reported in Refs. [15,17] were found to form another new band which is presented as a candidate chiral partner band.

II. RESULTS

High spin states in ^{140}Eu were populated following the reaction ^{92}Mo(^{51}V, $2pn$) at a beam energy of 205 MeV, the target consisting of two stacked 700 μg cm^{-2} foils. The beam was provided by the ESTU tandem accelerator at the Wright Nuclear Structure Laboratory at Yale University. Prompt decay γ rays were measured using the YRAST Ball detector array [18]. For this experiment, YRAST Ball consisted of seven Compton suppressed segmented clover germanium detectors [19] mounted at 90° with respect to the beam axis, each with $\sim$150% efficiency relative to a standard 3×3 inch NaI(Tl) detector. In addition, 16 Compton suppressed coaxial Ge detectors, each with $\sim$25% relative efficiency, were mounted in three rings at 50° (six detectors), 126° (eight detectors), and 160° (two detectors) with respect to the beam direction. For additional sensitivity to low energy γ rays and x rays, three LEPS detectors were also mounted in the array, two at 50° and one at 90°. The total photopeak efficiency of YRAST Ball in this configuration is about 2.5%.

The bombardment energy of 205 MeV was chosen following an earlier excitation function measurement where the beam energy was varied from 190 to 220 MeV. The yield of several high intensity transitions from ^{140}Gd, another three-particle ($p2n$) evaporation channel whose level scheme is well known, was optimal at 205 MeV. At this energy, about 15% of the reaction intensity went into ^{140}Eu, with the strongest population going into the nucleus ^{140}Gd. In a five-day experiment a total of 1.0×10^9 unfolded double and 4.7×10^8 unfolded triple coincidences were measured using YRAST Ball.

The level scheme of ^{140}Eu deduced from this data set is presented in Fig. 1. The level scheme was constructed using both triples and doubles γ coincidence data with the Radware analysis software [20]. The use of triples coincidences gives a decided advantage over doubles as many of the transitions in ^{140}Eu are similar in energy to transitions that occur with significant intensity in other neighboring nuclei, and single gates placed on these transitions are inevitably strongly polluted. To illustrate the quality of the triples data, some typical double-gated spectra are presented in Figs. 2–4. Details of these spectra will be discussed below. The measured γ ray transition energies and total intensities, together with the extracted directional correlation of oriented states (DCO) ratios, angular distributions, and Compton asymmetries for transitions in ^{140}Eu are presented in Table I. In general, the centroid values for the transition energies were determined using the doubles coincidence data and only when uncontaminated gates were not available, using the triples coincidences. The intensities in Table I are presented as relative intensities, with the intensity of the 640.6 keV transition defined as 100.

Transition multipolarities were determined following angular distribution, angular correlation and γ-ray polarization

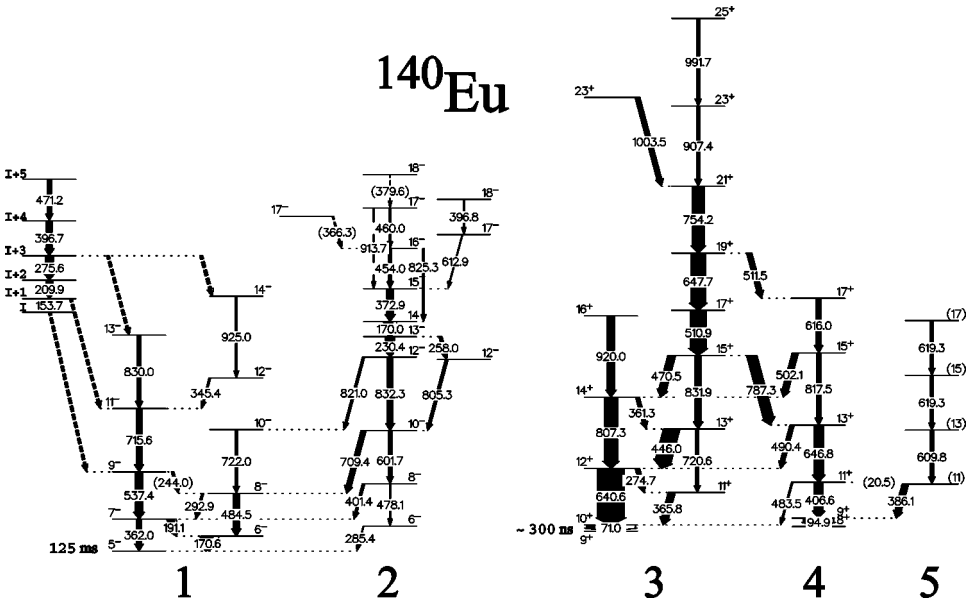

FIG. 1. Level scheme of ^{140}Eu from the present work. The widths of the arrows represent the total transition intensity.

analyses. For the angular distribution analysis, the four detector angles of YRAST Ball, 160°, 125°, 90°, and 50° with respect to the beam axis, were used. Due to the frequent occurrence of overlapping peaks and the weak intensity of others, a gated angular distribution analysis was utilized. For this analysis, the data were sorted into four coincidence matrices of E(any) versus $E(\theta)$. Here E(any) refers to a transition measured at any array position while $E(\theta)$ refers to a coincident transition measured at a specific angle. Coincidence gates were placed on transitions on the E(any) axis and the intensities of the transitions of interest were measured in the resulting spectra. This analysis assumes that any correlations present in the data are averaged out by the use of many coincidence pairs, an assumption that was verified by measuring the angular distributions of known quadrupole and dipole transitions in neighboring nuclei. The efficiency corrected intensity values were fit to the Legendre polynomial function: $W(\theta)=A_0+A_2P_2(\cos\theta)$. As $W(\theta)$ is symmetric about 90°, the 50° and 126° YRAST Ball detector angles provide approximately the same information to the fit, and can be used as a consistency check. The results, given as the ratio $a_2=A_2/A_0$, are presented in Table I. The a_2 values are also presented in Fig. 5 together with a weighted average of a_2 values from known transitions in ^{137}Sm, −0.15(6) for

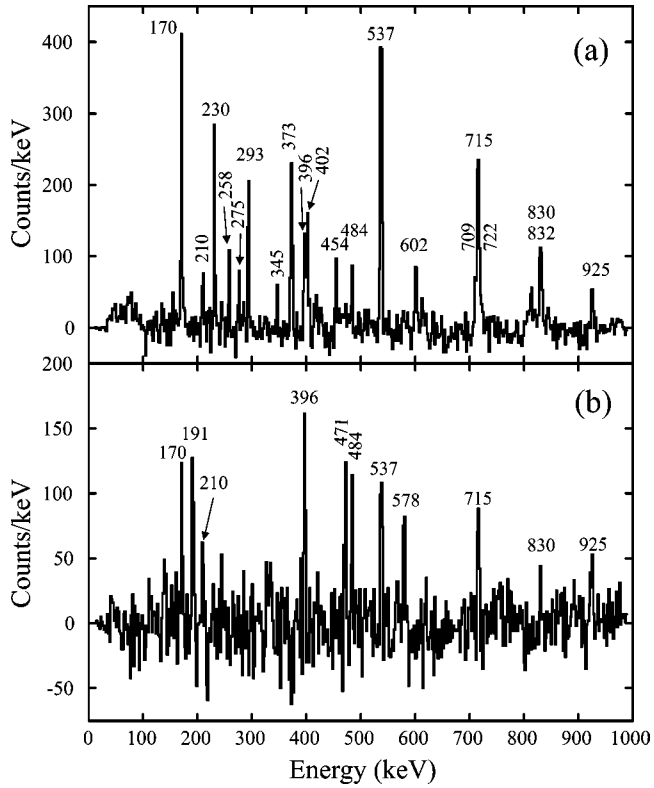

FIG. 2. (a) Double gate on the 170 and 191 keV transitions. (b) Double gate on the 345 keV transition and any of the 170, 191, 362, 537, 716 keV transitions in band 1.

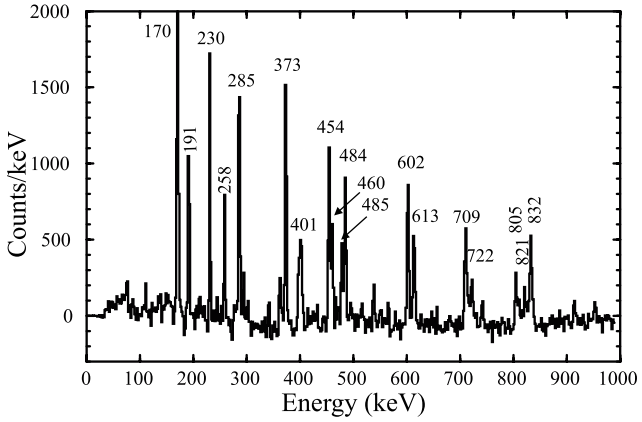

FIG. 3. Double gate on all transitions in band 2 from the 6^- to the 15^- levels. Self-coincidences are not included. Transitions in both bands 2 and 1 are clearly visible.

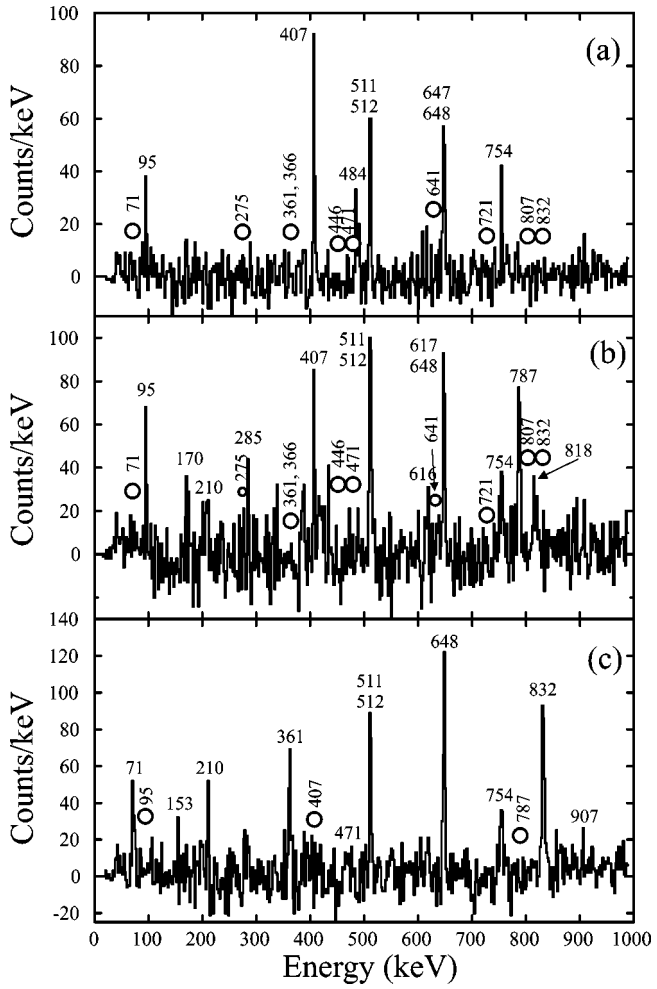

FIG. 4. (a) Double gate on the 647 keV doublet and 787 keV transition. Low-lying transitions in band 4 and high-lying transitions in band 3 are clearly visible. The energies of low-lying transitions in band 3 that are not in coincidence are indicated with circles. (b) Double gate on the 647 keV doublet and either the 407 or 95 keV band 4 transitions. The 787 keV transition linking bands 3 and 4 is very intense and the low-lying band 4 transitions and high-lying band 3 transitions are visible. Once again, circles indicate low-lying band 3 transitions that are not seen in coincidence. (c) Double gate on the 641 and 446 keV transitions in band 3. High-lying members of band 3 are clearly seen. The energies of the low-lying intense members of band 4 that are not in coincidence are indicated with circles.

known dipole and 0.38(7) for known quadrupole transitions.

A DCO analysis was also used to aid in the assignment of transition multipolarities. For this analysis the 90° and 160° detector rings were utilized, the data being sorted into a $E(90°)$ versus $E(160°)$ coincidence matrix. The DCO ratios were established by measuring the intensity of γ_1 at 90° when gated by γ_2 at 160°, divided by the intensity of γ_1 at 160° gating on γ_2 at 90°, that is, $R = I[\gamma_1(90°), \text{gate } \gamma_2(160°)]/I[\gamma_1(160°), \text{gate } \gamma_2(90°)]$. Results of the DCO analysis are presented in Table I and are summarized in Fig. 6. For comparison, weighted averages from several measured DCO ratios for known dipole and quadrupole transitions from ^{137}Sm, ^{138}Sm, ^{138}Eu, and ^{141}Gd are also included in Fig. 6. When corrected for the efficiency of both the gating and coincident transitions, ratios of R_{DCO} $\sim$0.90(4) and $\sim$0.62(2) [$\sim$1.71(8) and $\sim$0.85(2)] are found for the known $\Delta I=1$ and $\Delta I=2$ transitions, respectively, when gating on a $\Delta I=1(\Delta I=2)$ transition.

The polarization sensitivity of the YRAST Ball clover detectors [19] helped in the assignment of the electromagnetic character of the transitions. The Compton asymmetry ratio, defined as $A=(N_{\parallel}-N_{\perp})/(N_{\parallel}+N_{\perp})$, is sensitive to the polarization of the γ rays, where $N_{\parallel}(N_{\perp})$ is the number of added-back photopeak counts which scatter between two elements of a clover detector parallel (orthogonal) to the beam-γ plane. For this definition, purely magnetic transitions have positive values of A while purely electric transitions have negative values of A. Extracted values for the asymmetry ratio A are summarized in Fig. 7 and Table I for many of the transitions assigned to ^{140}Eu. The Compton asymmetry was also extracted for several known $M1$ and $E2$ transitions from the neighboring nuclei ^{137,138}Sm. The weighted averages for these transitions, 0.09(2) and −0.06(1), respectively, are included in Fig. 7 for comparison.

As mentioned above, the low lying structure of ^{140}Eu is characterized by two isomeric states, a long lived (125 ms) 5^- isomer at an excitation energy of 185.3 keV and a recently identified, higher-lying, $\sim$300 ns isomer [16] linked to the 5^- isomer via several intermediate levels and transitions. In the present experiment, the recoil velocity of the ^{140}Eu nuclei was $v/c\sim3\%$ or $\sim$9 mm per ns. Thus the experiment is not sensitive to the γ rays directly depopulating the isomeric levels known in this nucleus, but prompt feeding which bypasses the isomeric states may be observed. The 170, 191, 361, and 285 keV transitions identified in the isomer decay tagging experiment [16], and connecting levels intermediate between the two isomers, were seen both in the present work and the excitation function measurement, confirming their assignment to ^{140}Eu. Several more transitions were assigned through coincidences with these γ-rays.

Band 1, shown on the left-hand side of Fig. 1, was placed directly feeding the 5^- isomer [17]. The lower part of band 1 consists of a series of four $\Delta I=1$ $M1/E2$ transitions with crossover $\Delta I=2$ $E2$ transitions. The intense 170.6 and 191.1 keV transitions (visible in the total projection) and the weaker 362.0 keV crossover transition are identified with the 170, 191, and 361 keV transitions that directly populate the 5^- isomeric level in Ref. [16]. At higher spins, the decay intensity in band 1 is carried by $E2$ transitions with weak or unobserved dipole transitions. The $\sim$170 keV transition is a doublet, the second member of which, 170.0 keV, is placed in band 2. A double gate placed on the 191.1 and $\sim$170 keV transitions, Fig. 2(a), shows the doublet character of the 170 keV transition, the expected strong coincidences with other transitions in band 1, and the higher lying transitions in band 2. The 362.0, 537.4, 715.6, and 830.0 keV transitions were also reported in Ref. [17]. However, the higher lying $15^-\rightarrow13^-$ 843 keV transition in Ref. [17] could not be confirmed in the present work. The probable signature partner band, consisting of the 484.5 and 722.0 keV $E2$ transitions together with the connecting $\Delta I=1$ transitions (244.0 and 292.9 keV), is reported here for the first time. The

TABLE I. Summary of our results for ^{140}Eu. The columns show the transition energy in keV, the intensity relative to the 640.6 keV transition, the Compton asymmetry ratio A, the angular distribution a_2 value, the DCO ratio, the multipolarity of the gate used to measure the DCO ratio, and finally the assigned multipolarity of the observed transition in ^{140}Eu.

E_γ (keV)	Intensity[a]	$A=\frac{N_\parallel - N_\perp}{N_\parallel + N_\perp}$	a_2	*DCO*	Gate[b]	Multipolarity[c]
71.0(2)	>130[d]		0.55(55)[d]	2.83(98)[d]	*q*	(*M*1/*E*2)
94.9(2)	≥65[d]		0.57(23)[d]	1.25(42)[d]	*q*	(*M*1/*E*2)
153.7(2)	33		0.36(24)	0.88(29)	*d*	*M*1/*E*2
170.0(2)	39(7)					(*M*1/*E*2)
170.6(1)	72	0.16(21)		1.33(9)	*q*	*M*1/*E*2
191.1(2)	35	0.16(8)	0.14(8)	1.23(7)	*q*	*M*1/*E*2
209.9(2)	26		0.00(19)	0.96(33)	*d*	*M*1/*E*2
230.4(1)	34	0.16(5)		0.73(4)	*d*	*M*1/*E*2
244.0(2)	≥8			1.59(75)	*d*	*M*1/*E*2
258.0(2)	12	0.16(7)		1.00(12)	*d*	*M*1/*E*2
274.7(3)	16	0.11(12)		1.49(82)	*q*	*M*1/*E*2
275.6(2)	31	0.29(13)	−0.21(26)	0.96(21)	*d*	*M*1/*E*2
285.4(3)	>3	0.13(9)	0.09(12)	0.78(10)	*d*	*M*1/*E*2
292.9(4)	>15	0.37(11)	0.08(21)	1.02(20)	*d*	*M*1/*E*2
345.4(3)	4			1.37(41)	*q*	*M*1/*E*2
361.3(2)	16	0.09(9)	−0.23(23)	0.63(10)	*d*	*M*1/*E*2
362.0(2)	20	0.11(14)		1.02(9)	*q*	*E*2
365.8(3)	26	0.02(12)	−0.11(28)	1.78(37)	*q*	*M*1/*E*2
366.3(2)	4					
372.9(2)	25	0.13(3)		1.45(9)	*d*	*M*1/*E*2
379.6(2)	1					
386.1(2)	24	−0.16(23)	0.13(14)	0.99(30)	*q*	*E*2
396.7(2)	22	0.12(8)	−0.10(23)	1.29(17)	*d*	*M*1/*E*2
396.8(2)	3					
401.4(2)	>9	0.04(8)	−0.16(9)	1.45(18)	*d*	*M*1/*E*2
406.6(2)	>33	−0.01(7)	0.46(19)	0.93(16)	*q*	*E*2
446.0(1)	59	−0.01(3)	−0.10(14)	1.77(11)	*q*	*M*1/*E*2
454.0(2)	10	0.21(8)	−0.34(21)	2.04(47)	*d*	*M*1/*E*2
460.0(3)	6		0.20(28)	1.41(41)	*d*	*M*1/*E*2
470.5(2)	28	0.16(11)		3.4(6)	*q*	*M*1/*E*2
471.2(3)	14	0.09(7)	0.18(81)			*M*1/*E*2
478.1(4)	>3			0.61(15)	*d*	*E*2
483.5(4)	5			1.9(1.0)	*q*	*M*1/*E*2
484.5(2)	>20	−0.04(4)		0.69(4)	*d*	*E*2
490.4(3)	16	0.17(9)	−0.46(46)	2.7(9)	*q*	*M*1/*E*2
502.1(4)	23		0.35(36)	2.14(50)	*q*	*M*1/*E*2
510.9(2)	58			0.98(14)	*q*	*E*2
511.5(3)	<19	0.03(6)				(*E*2)
537.4(1)	28	−0.05(4)		0.78(5)	*d*	*E*2
601.7(2)	>14	−0.007(41)	0.23(16)	0.87(6)	*d*	*E*2
609.8(4)	13			1.14(38)	*q*	*E*2
612.9(5)	8	0.11(6)	−0.23(18)	1.5(3)	*d*	(*E*2)
616.0(5)	19					(*E*2)
619.3(3)	≈10			1.51(32)	*q*	*E*2
640.6(1)	≡100	−0.12(5)		1.02(9)	*q*	*E*2
646.8(3)	35(24)					(*E*2)
647.7(2)	53	−0.03(6)		0.87(14)	*q*	*E*2
709.4(4)	>22	−0.01(11)		0.76(8)	*d*	*E*2
715.6(2)	21	−0.08(4)		1.01(7)	*q*	*E*2

TABLE I. (*Continued.*)

E_γ (keV)	Intensity[a]	$A=\frac{N_\parallel - N_\perp}{N_\parallel + N_\perp}$	a_2	*DCO*	Gate[b]	Multipolarity[c]
720.6(2)	10			0.49(10)	*d*	*E*2
722.0(3)	>10			0.63(6)	*d*	*E*2
754.2(3)	44	−0.07(9)	0.58(30)	0.88(12)	*q*	*E*2
787.3(3)	38	−0.06(7)	0.45(27)	1.06(10)	*q*	*E*2
805.3(3)	>12	−0.07(11)		0.59(9)	*d*	*E*2
807.3(2)	5	−0.11(4)	0.53(17)	1.22(16)	*q*	*E*2
817.5(5)	20(10)	−0.13(14)		1.12(21)	*q*	*E*2
821.0(3)	>10	−0.07(12)		2.53(74)	*d*	*E*2
825.3(1.5)	7					(*E*2)
830.0(3)	15			0.92(17)	*q*	*E*2
831.9(3)	30	−0.12(9)	0.34(13)	0.95(23)	*q*	*E*2
832.3(3)	>24	−0.11(6)		0.62(5)	*d*	*E*2
907.4(4)	13					(*E*2)
913.7(5)	3					
920.0(3)	27	−0.28(11)	0.72(41)	1.11(13)	*q*	*E*2
925.0(3)	4	−0.62(23)		0.82(18)	*q*	*E*2
991.7(4)	11					(*E*2)
1003.5(3)	18			1.32(40)	*q*	*E*2

[a]Intensity errors are ≈10% unless otherwise noted.
[b]Nature of gate used for DCO measurement: "stretched" dipole or "stretched" quadrupole.
[c]Multipolarity assigned to the transition.
[d]Array efficiencies for transitions below $E \approx 121.8$ keV are not well defined.

925.0 keV transition is seen in both the present work and in Ref. [17]. Figure 2(b), a double gate on the 345.4 keV transition and low lying members of band 1 shows that the 345.4 and 925.0 keV transitions are in coincidence with one another and members of band 1. We have placed these transitions with the 345.4 keV transition directly feeding the 11^- level of band 1, though the ordering of these two transitions is uncertain. The $12^- \rightarrow 10^-$ *E*2 transition is not observed.

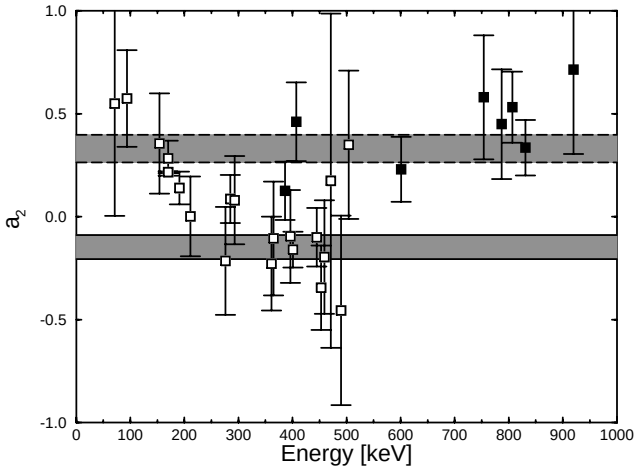

FIG. 5. Plot of extracted a_2 values from Legendre polynomial fits of angular distribution intensities. Open (filled) squares are assigned *M*1/*E*2 (*E*2) transitions. The solid (dashed) bounded region denotes weighted average and error of a_2 values extracted from known *M*1 (*E*2) transitions in neighboring nuclei. See text for details.

A small band consisting of a series of five $\Delta I=1$ transitions is shown beside band 1 in Fig. 1. These transitions are mutually coincident and are in coincidence with low lying transitions in band 1, though direct linking transitions have not been identified. The dashed lines in Fig. 1 indicate possible decay paths. As such, spin assignments are tentative and are given relative to the lowest level in the band. The transitions have been ordered such that the transition energies increase, and the total transition intensities decrease, with increasing spin. The exception in the intensity ordering is the lowest lying transition, 153.7 keV, which has less in-

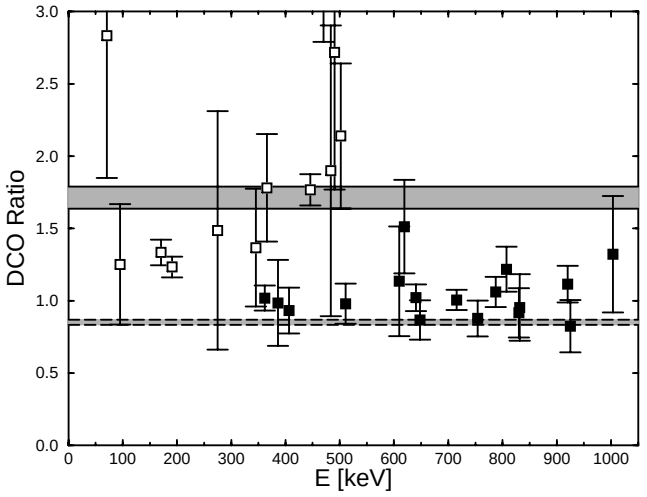

FIG. 6. Plot of the measured DCO ratios, gating on quadrupole transitions. Symbols are as in Fig. 5. See text for details.

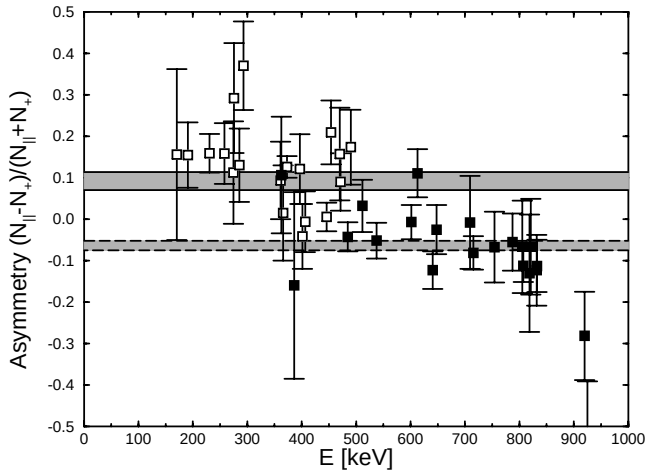

FIG. 7. Plot of polarization asymmetry ratios $A=(N_{\parallel}-N_{\perp})/(N_{\parallel}+N_{\perp})$. Symbols are as in Fig. 5. See text for details.

tensity than the 210.2 and 275.6 keV transitions presumably due to unobserved decay out transitions. These intensity measurements are complicated, since very intense mutually coincident γ rays with energies similar to the 210.2 and 275.6 keV transitions occur in ^{137}Sm, which is produced via the strongly competing αpn three particle evaporation channel.

Band 2, shown near the left in Fig. 1, is reported here for the first time. Band 2 is dominated by $\Delta I=2$ $E2$ transitions at lower spins. However, at spin $I\sim 12\hbar$, a band crossing occurs (see below) after which the nature of the band changes and dipole transitions dominate the decay with weak or unobserved $E2$ crossover transitions. A typical double gated spectrum for transitions in band 2 is presented in Fig. 3. Several weak branches, including the 612.9,396.8 keV sequence and the tentative 366.3 keV transition, feed into band 2 at higher spins. Two $\Delta I=2$ $E2$ transitions (821.0 and 709.4 keV) and two $\Delta I=1$ $M1/E2$ transitions (401.4 and 285.4 keV) connect levels in band 2 and band 1 allowing firm spin, parity, and excitation energy assignments for band 2. The 285.4 keV transition, assigned as a $\Delta I=1$ $M1/E2$ transition, feeds directly from the lowest observed level of band 2 to the 5^- isomeric level. Thus band 2 is assigned negative parity with the lowest observed level having a spin $I=6$. The 366.3 and 379.6 keV transitions are tentative, and are shown in Fig. 1 with dashed arrows.

Band 3, shown near the middle of Fig. 1, at lower spins consists of a sequence of six $\Delta I=1$ $M1/E2$ transitions with crossover $\Delta I=2$ $E2$ transitions. A band crossing occurs around spin $15\hbar$, after which the in-band decay is dominated by $\Delta I=2$ $E2$ transitions. The observed transitions in band 3, up to spin 25^+, confirm the band reported as $\pi h_{11/2}\otimes\nu h_{11/2}$ in Ref. [17]. Relative spin assignments were made following DCO, angular distribution, and Compton asymmetry measurements. Note that the spins reported here are two units higher than in Ref. [17]. Absolute spin assignments are based on a systematic study of level energies in the $\pi h_{11/2}\otimes\nu h_{11/2}$ bands in neighboring $N=73$, 75, and 77 nuclei [21]. The energies of the known $\pi h_{11/2}\otimes\nu h_{11/2}$ bands, relative to the 10^+ level, are plotted for odd-odd nuclei from $_{55}$Cs through $_{63}$Eu and for $N=73$ through 77, see Fig. 8. As can be seen for nuclei of the same Z, the level spacing increases as N increases from 73 to 77, approaching the closed neutron shell at $N=82$. In contrast, for the same N, the level spacing decreases as Z increases from 55 to 63, towards the proton midshell. The excitation energies for the $\pi h_{11/2}\otimes\nu h_{11/2}$ band in ^{140}Eu are plotted on the far right in Fig. 8 using the spin assignments from the present work (symbols connected with solid lines) and from Ref. [17] (symbols connected with dashed lines). Using these assignments, the excitation energies show a sudden upturn for the levels above the 10^+ level, and sudden downturn for the 9^+ level, contrary to the trends described. Since the energy difference between neighboring levels generally increases smoothly with spin, the relatively large difference in energy between neighboring levels for ^{140}Eu supports a revision of the spin assignments. The ^{140}Eu data, plotted with our spin assignments shown on the far

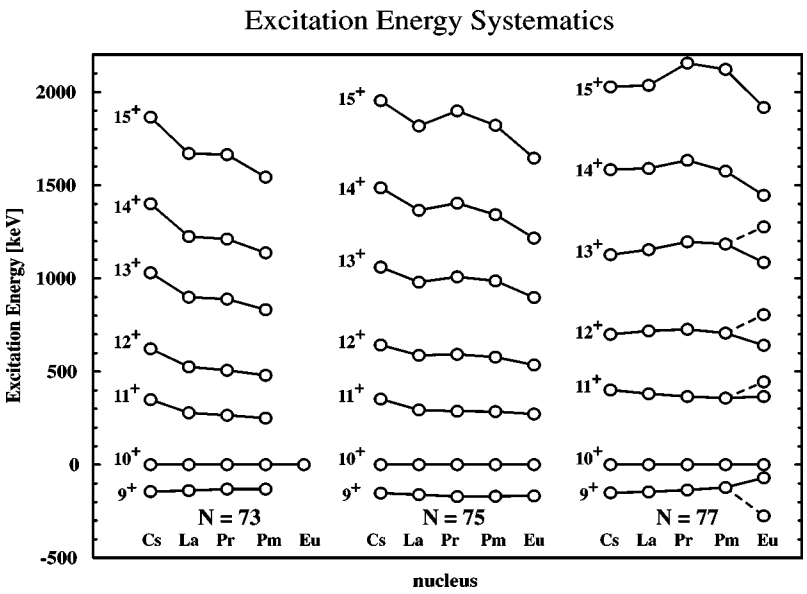

FIG. 8. Systematics of level energies in $\pi h_{11/2}\otimes\nu h_{11/2}$ bands in the mass 130 region as a function of proton number, plotted for several different neutron numbers. The level energies are plotted relative to the 10^+ level, following the level assignments of Liu *et al.* [21]. ^{140}Eu, with $N=77, Z=63$, lies at the far right. Level assignments of Cullen *et al.* [17] are connected with dashed lines. Level assignments from the current work are connected with solid lines.

right in Fig. 8, connected with solid lines, continue the trend of smoothly decreasing interlevel spacing with increasing Z, and follows the trend of larger interlevel spacing with increasing N. In addition, a 71.0 keV transition not observed in Ref. [17] was placed at the bottom of band 3 as a new $10^+ \rightarrow 9^+$ transition. The 71.0 keV transition is clearly visible in Fig. 4(c), a double gate on the 640.6 and 446.0 keV transitions in band 3. It is similar in energy to the low energy $10^+ \rightarrow 9^+$ transitions seen in other nuclei in the systematics plot, further supporting its placement and spin assignments.

Curiously, the low-lying, even-spin levels in band 3 are populated more strongly than the odd spin levels. The 720.6 and 831.9 keV $E2$ transitions (connecting the odd-spin low-lying levels) are less intense than the 640.6, 807.3, and 920.0 keV $E2$ transitions. Nevertheless, it is the odd-spin signature partner member of this band that is observed to higher spins ($25\hbar$ compared to $16\hbar$), indicating that the even-spin levels must lie higher in energy following the band crossing. The $16^+ \rightarrow 14^+$ 920.0 keV transition confirms the 920 keV transition reported in Ref. [17]. The odd spin sequence reported here agrees with the results of Ref. [17] up to the 991.7 keV transition. We were unable to confirm the 962, 890, and 1074 keV transitions seen in that reference.

Due to its similarity of level energies as a function of spin in bands 3 and 4, band 4 is of considerable interest. The 94.9, 406.6, 646.8, and 787.3 keV transitions were previously reported in Ref. [17], where they were placed as a side feeding cascade, above and in coincidence with the 754.2 keV transition of band 3. While their coincidence with the 754.2 keV transition is confirmed in our experiment, a triples coincidence analysis indicates that the transitions are considerably lower in the level scheme and form a band, as presented in Fig. 1. In particular, the 787.3 keV transition is not in coincidence with any of the transitions lying between the 15^+ and 12^+ levels in band 3, placing it parallel to these levels. This can be seen in Fig. 4(a), a double gate on the 787.3 and 646.8 keV transitions. Furthermore, the 406.6 and 94.9 keV transitions are not in coincidence with any band 3 member below the 15^+ level, see Fig. 4(b). Finally, Fig. 4(c) shows a double gate on the 446.0 and 640.6 keV band 3 transitions. No evidence is seen in this spectrum for the low lying and most intense band 4 members. The observation of the 502.1, 490.4, and 483.5 keV linking transitions confirms our placement. Most of the intensity of band 4 comes from band 3 via the 787.3 keV linking transition. Within band 4, the dashed 817.5 keV transition weakly links the 616.0 keV transition as part of the same band. The 502.1 keV transition feeds from directly below the 616.0 keV transition to band 3 and takes some of the intensity away from band 4. The $\sim$647 keV transition is a doublet, occurring as 646.8 keV in band 4 with the stronger partner occurring as 647.7 keV in band 3. Thus, coincidences with this transition bring back too much background to clearly see the 817.5 keV transition. However, the 817.5 keV transition is seen in double gated coincidence spectra gated by the 616.0 and 406.6 keV transitions.

DCO analysis, Compton asymmetries, and angular distribution measurements show that band 4 comprises transitions that are either of $\Delta I=1$ mixed $M1/E2$ character or of $\Delta I=2$ $E2$ character, and is connected to band 3 by $E2$ (787.3 and 511.5 keV) and mixed $M1/E2$ (502.1, 490.4, and 483.5 keV) transitions. The comparable strength of intraband and interband transitions in and between bands 3 and 4 supports the assignment of the interband transitions as $\Delta I=1$ $M1/E2$ and $\Delta I=2$ $E2$. The parity conserving character of both the $M1/E2$ and $E2$ interband transitions suggest a total positive parity configuration for band 4.

Finally, band 5, shown on the right side of Fig. 1, consists of a series of three $\Delta I=2$ transitions, 609.8, 619.3, and 619.3 keV, which are strongly in coincidence with both the 94.9 keV transition of band 4 and the 386.1 keV, probably $\Delta I=2$ transition. The 386.1 keV transition is easily seen in double coincidence gates placed on the 94.9 and 646.8 keV transitions, and is placed at the bottom of the band. The 609.8 keV and 619.3 keV doublet are strongly in coincidence with the 386.1 and 94.9 keV transitions, but are not in coincidence with any other transitions identified in ^{140}Eu. A very low energy 20.5 keV transition connecting the 646.8 and 386.1 keV transitions is implied by the coincidence of the 646.8 and 386.1 keV transitions, although the 20.5 keV transition has not been observed. The 20.5 keV transition must be fast enough for the 646.8 and 386.1 keV transitions to both occur in the sensitive region of the array, a concern since transition half-lives are inversely dependent on transition energy. Calculated Weisskopf single particle estimates for the 20.5 keV transition half-life are 30 ps and 3 ns for $E1$ and $M1$ transitions, respectively, fast enough to be observed in the present experiment. The large electron conversion coefficient for this low energy transition ($\alpha \sim 100$ for $M1$ and ~ 10 for $E1$ transitions [22]) and the low sensitivity of the detector array at this low energy, leaves the 20.5 keV transition as only conjectural. The ordering of the other transitions in band 5 is based on intensity arguments.

III. DISCUSSION

To investigate the nature of these bands, we performed TRS calculations for ^{140}Eu. These calculations, for essentially any low-lying proton and neutron orbital combinations, predict a γ soft potential energy surface with two potential energy minima, at a deformation of $\beta \sim 0.2$ and $\gamma \sim \pm 25°$, see Fig. 9. As previously mentioned, such minima open up the interesting possibilities of chiral twin bands and/or shape coexisting bands occurring in ^{140}Eu. These minima persist over a wide frequency range from $\hbar\omega=0$ to $\sim$0.450 MeV, corresponding to a spin of $I \sim 24\hbar$. These minima are close in energy, to frequencies of at least $\hbar\omega \sim 0.450$ MeV, and spin $\sim 24\hbar$ for both low lying positive and negative parity configurations. For these deformations, proton orbitals close to the Fermi surface include the above mentioned negative parity $h_{11/2}$ orbitals, originating from the low-Ω [541]3/2 Nilsson configuration, and the (highly mixed) positive parity $d_{5/2}$ [411]3/2 and $g_{7/2}$ [413]5/2 orbitals. For neutrons, the orbitals close to the Fermi surface include the negative parity $h_{11/2}$ orbital from the high-Ω [505]11/2 orbital and the positive parity $d_{3/2}$ [400]1/2 orbital.

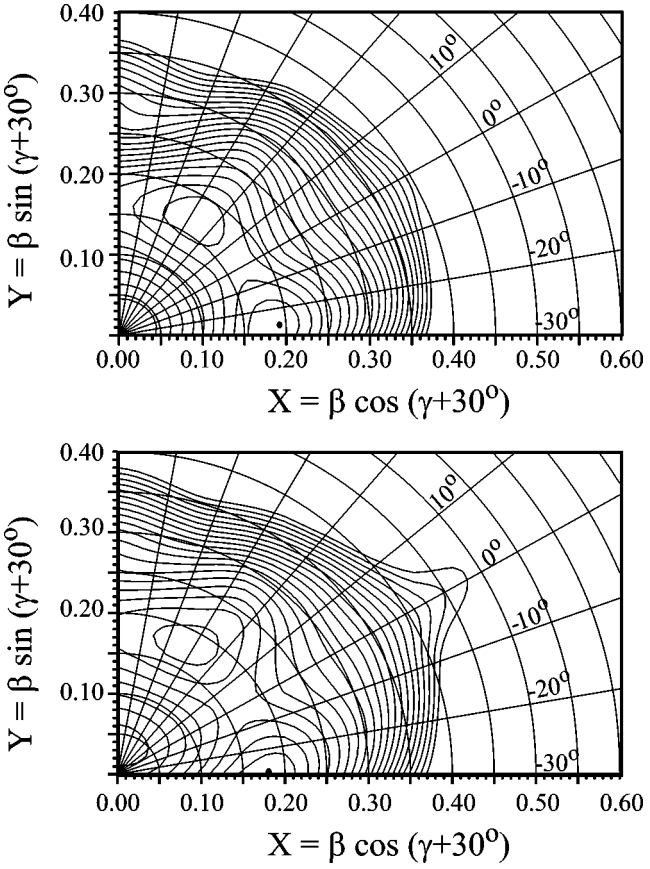

FIG. 9. Polar coordinate plots of total Routhian surface (TRS) calculations at $\hbar\omega$=0.2 MeV. Radial length is β deformation, angle is γ deformation. The top figure is for proton (π,α)=neutron (π,α)=$(-,-1/2)$, which describes the $\pi h_{11/2}\otimes\nu h_{11/2}$ configuration. The bottom figure is for proton (π,α)=$(+,+1/2)$, neutron (π,α) =$(-,-1/2)$, which describes the $\pi(d_{5/2},g_{7/2})\otimes\nu h_{11/2}$ configuration. There are potential energy minima in both plots for $\beta\sim0.2,\gamma\sim+25°$ and $-25°$. Contours are 175 keV.

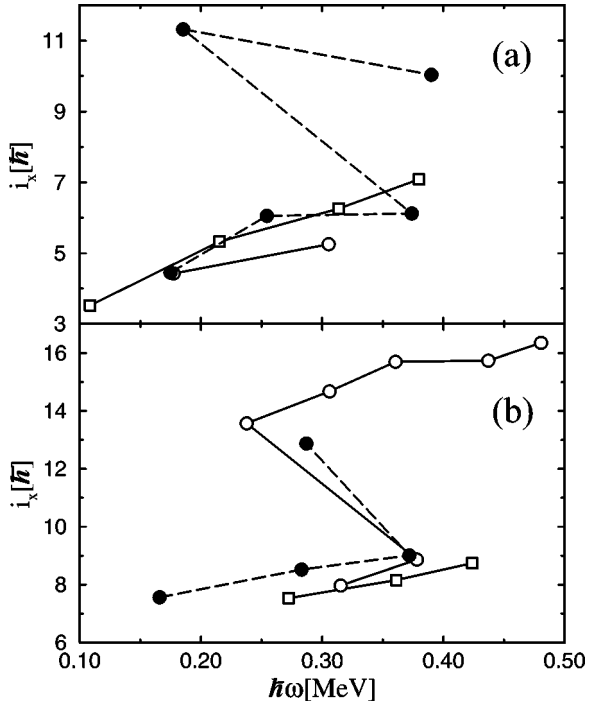

FIG. 10. (a) Alignment plot of bands 1 and 2. Squares denote transitions between odd spin levels, circles between even spin levels. The open figures are for band 1 while the closed symbols are for band 2. (b) Alignment plot of bands 3 and 4. Squares denote transitions between odd spin levels, circles between even spin levels. Open figures are for band 3, closed symbols are for band 4.

A. The negative parity bands

We consider first the negative parity bands, bands 1 and 2. The aligned angular momenta for bands 1 and 2 are plotted in Fig. 10(a) as a function of rotational frequency. The Harris parameters used, J_0=5$\hbar^2$ MeV^{-1} and J_1=45$\hbar^4$ MeV^{-3}, were chosen to subtract the angular momentum of the core. For band 1, no backbend is observed through the highest transitions identified, while band 2 shows a sharp backbend centered at $\hbar\omega\sim$0.28 MeV, with $\Delta i_x\sim6\hbar$. As particles in the intruder $h_{11/2}$ orbitals have the largest angular momentum in this mass region, they are the most probable particles participating in the pair alignment. The large increase in alignment of $\Delta i_x\sim6\hbar$ observed in Fig. 10(a) is consistent with the angular momentum gain from the alignment of a pair of $h_{11/2}$ particles.

Quasiparticle Routhian calculations [23] performed for the deformation β_2=0.19, β_4=−0.021, and γ=−26° are presented in Fig. 11. As can be seen, the lowest frequency for a band crossing is calculated to be $\hbar\omega\sim$0.32 MeV, corresponding to the alignment of a pair of $h_{11/2}$ protons, in good agreement with the experimental alignment plot for band 2. The presence of the *AB* $\pi h_{11/2}$ crossing suggests that the proton configuration for band 2 below the backbend does not involve the $\pi h_{11/2}$ orbital. The probable orbital configurations then are either proton $d_{5/2}$[411]3/2 or $g_{7/2}$[413]5/2 coupled to an $h_{11/2}$[505]11/2 neutron. Following the Gallagher-Moszkowski rules for coupling of single particle angular momenta, the likely $K(=\Omega_\pi\pm\Omega_\nu)$ for the band is 6 for the $\pi d_{5/2}\otimes\nu h_{11/2}$ band and 2 for the $\pi g_{7/2}\otimes\nu h_{11/2}$ band [24]. It is misleading though to describe band 2 as solely $\pi d_{5/2}\otimes\nu h_{11/2}$ or $\pi g_{7/2}\otimes\nu h_{11/2}$ due to the mixing which is likely to occur between the two proton orbitals.

The $\pi h_{11/2}$ orbital coupled to the low-lying neutron $d_{3/2}$ orbital is the most probable configuration for the negative parity states at low spin, below the 5^- isomer [16]. That said, the negative parity configurations above the 5^- isomer probably do not include the $d_{3/2}$ neutron orbital. The lowest lying total negative parity configuration at higher spins is calculated to be mixed $\pi(g_{7/2},d_{5/2})\otimes\nu h_{11/2}$. Thus, one possibility is that both band 1 and band 2 involve the $\pi(g_{7/2},d_{5/2})\otimes\nu h_{11/2}$ configuration. In Ref. [17], the band that we have labeled as band 1 is assigned the $\pi h_{11/2}\otimes\nu g_{7/2}$ configuration in Fig. 5 and the $\pi h_{11/2}\otimes\nu d_{5/2}$ configuration in the text, both of which we consider to be less likely.

The ΔI=1 sideband shown to the left of band 1 is intriguing. Though the specific linking transitions could not be identified, the band is in coincidence with band 1. Furthermore, it is tantalizingly similar to the high spin portion of band 2. The similarity of the behavior leads one to speculate that these transitions form a continuation of band 1 after a

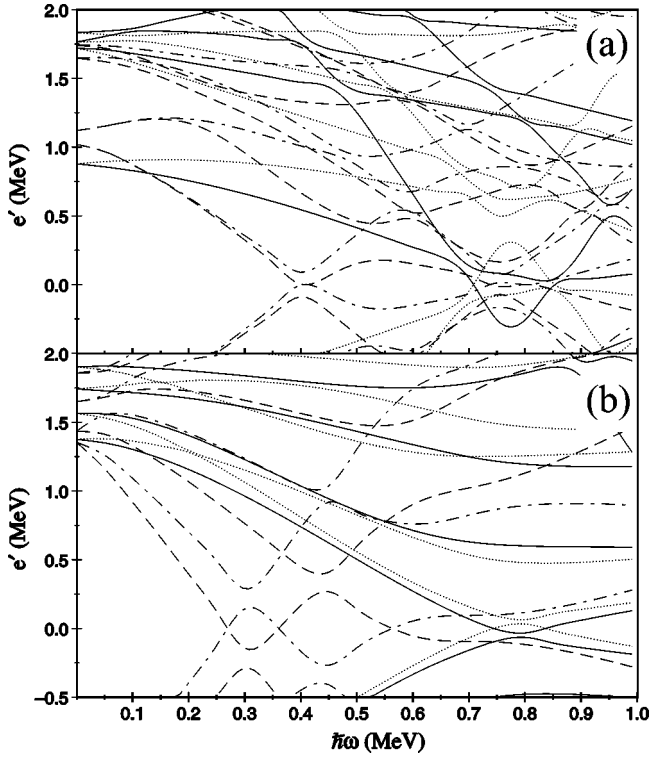

FIG. 11. Calculated Woods-Saxon quasiparticle Routhian plot for $N=77, Z=63$. The parity and signature (π, α) of the orbitals are represented by solid lines (+, +1/2), dotted lines (+, −1/2), dot-dash lines, (−, +1/2), dashed lines (−, −1/2). The deformation chosen for the calculations is $\gamma\sim-25°$, from TRS calculations. (a) Plot for neutron configurations. (b) Plot for proton configurations.

band crossing, similar to that observed in band 2. Further experiments are required to clarify the structure of the bands and determine if there is a sharp backbend in band 1. These bands and their possible interpretations will be discussed further below.

B. The positive parity bands

We now turn to a discussion of the positive parity bands. Band 3 is the yrast band based on the $\pi h_{11/2}\otimes\nu h_{11/2}$ orbital configuration [15,17]. Strongly populated yrast bands based on a $\pi h_{11/2}\otimes\nu h_{11/2}$ configurations are well known in neighboring odd-odd nuclei, see Fig. 8. In addition, our quasiparticle Routhian calculations suggest that both the proton and neutron $h_{11/2}$ orbitals lie near the Fermi surface for $N=77, Z=63$ at the calculated deformation. As previously mentioned, a systematic comparison of the energy levels in band 3 with those of $\pi h_{11/2}\otimes\nu h_{11/2}$ double intruder bands from neighboring $N=73, 75, 77$ nuclei strongly suggests a $\pi h_{11/2}\otimes\nu h_{11/2}$ positive parity configuration for band 3, confirming the assignment of Ref. [17].

The orbital configuration of band 4 can be deduced from its relation to band 3. Band 4 is linked to band 3 by several transitions. The measured DCO ratio, angular distribution a_2 value, and Compton asymmetry ratio A for the intense 787.3 and 490.4 keV transitions establish them to be parity conserving $E2$ and $M1/E2$ transitions, respectively. The results for the other two linking transitions, the 502.1 and 483.5 keV transitions, are more ambiguous, though consistent with their assignment as $M1/E2$ transitions. Thus, band 4 is assigned the same positive parity as band 3. Moreover, for both the proton and neutrons, the $h_{11/2}$ orbitals are intruder orbitals and are the only negative parity orbitals near the Fermi surface. The possible configurations for band 4 then are either the total positive parity $\pi h_{11/2}\otimes\nu h_{11/2}$ orbital configuration or a combination of proton and neutron orbitals that are individually positive parity. The selection rules for $M1$ and $E2$ transitions make it exceedingly unlikely that both proton and neutron configurations are changed in a single transition, and so band 4 is assigned the same $\pi h_{11/2}\otimes\nu h_{11/2}$ orbital configuration as band 3.

Further evidence for this configuration assignment is provided in the alignment plot of bands 3 and 4, presented in Fig. 10(b), where one observes the same large initial aligned angular momentum for the bands ($i_x\sim7\hbar$), consistent with $\pi h_{11/2}\otimes\nu h_{11/2}$ assignment. Band 3 [open points in Fig. 10(b)] backbends at a frequency of $\hbar\omega\sim0.31$ MeV. Band 4 (solid points) is not observed to high enough energies to complete its backbend, but both bands 3 and 4 begin to align at the same frequency, $\hbar\omega\sim0.37$ MeV. Cranked shell model calculations for $\beta\sim0.2$, $\gamma\sim+25°$ and $\beta\sim0.2$, $\gamma\sim-25°$, (see Fig. 11) predict the second $h_{11/2}$ band crossing at $\hbar\omega\sim0.45$ MeV for negative γ deformation, but at only $\hbar\omega\sim0.35$ MeV for positive γ deformation. The lower value is in good agreement with experimental results.

While the calculated and experimental alignment frequencies are not in exact agreement, it is instructive to look at regional trends. To view these trends, experimental alignment plots of the $\pi h_{11/2}\otimes\nu h_{11/2}$ bands in the doubly odd nuclei $_{57}$La, $_{59}$Pr, $_{61}$Pm, and $_{63}$Eu, for $N=75$ and $N=77$, are presented in Fig. 12. The same Harris parameters, $J_0=5\hbar^2$ MeV^{-1} and $J_1=45\hbar^4$ MeV^{-3}, which were chosen to subtract out the average core rotation for the ^{140}Eu, are used in all the plots (this explains the slow increase in the plotted alignment in the $N=73$ isotopes). Several of the nuclei show experimental evidence of band crossing, with a gain in single particle angular momentum i_x of $\sim6\hbar$, consistent with the alignment of a pair of $h_{11/2}$ protons. Looking at the well studied $N=75$ isotones, we see a clear decrease in the crossing frequency as proton number increases, from $\hbar\omega\sim0.47$ MeV for Pr to 0.39 MeV for Eu. This can be seen in Fig. 12, with the open data points representing the yrast bands. The closed points, the chiral partner bands, are similar in behavior to the yrast bands. For the $N=73$ isotones backbends are not observed. However, the same trend is present in the decreasing frequency of the start of the backbend for these isotones, from >0.5 MeV in La to ~0.4 MeV in Pm. No information is available for the $N=73$ ^{136}Eu. A lowering in the alignment frequency is consistent with a decrease in deformation as a function of proton number, and this trend would be expected to continue with the $N=77$ isotones. The La alignment frequency for $N=77$ already occurs at $\hbar\omega\sim0.4$ MeV. Given the systematics, it is expected that the $N=77$ ^{140}Eu backbend would occur at a frequency lower than $\hbar\omega\sim0.4$ MeV. The absence of evidence for a backbend in the ^{136}Pr and ^{138}Pm nuclei is anomalous, and might be re-

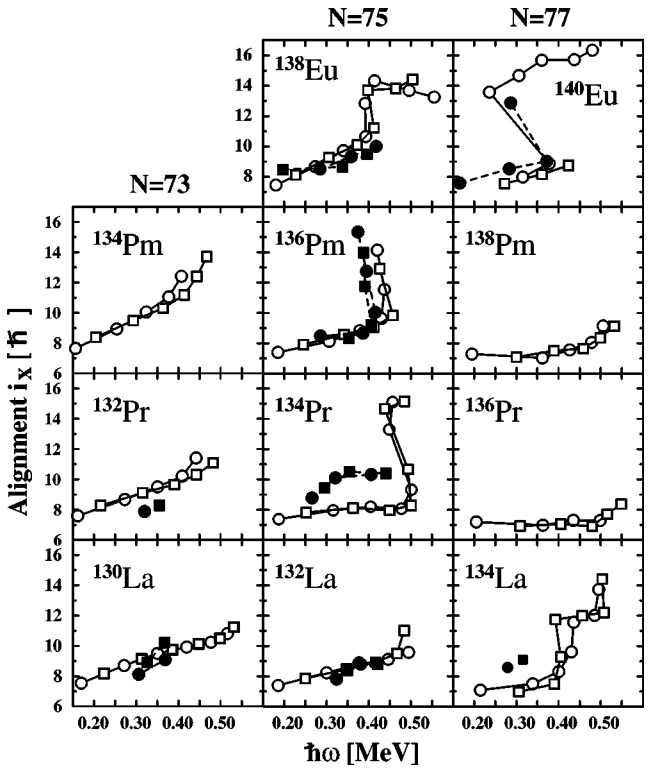

FIG. 12. Systematics of alignments of known $\pi h_{11/2} \otimes \nu h_{11/2}$ bands in doubly odd nuclei from N=73 to 77 and Z=57 to 63. Squares denote even spin levels, circles odd spin levels. Open figures are for the more strongly populated main band, closed symbols denote the side chiral partner band. The Harris parameters $J_0 = 5\hbar^2$ MeV^{-1} and $J_1 = 45\hbar^4$ MeV^{-3}, and K=6, were used for all plots for convenience.

solved with an experimental observation of transitions at higher spins. In conclusion, it is most likely for both bands 3 and 4 to have a $\pi h_{11/2} \otimes \nu h_{11/2}$ configuration.

As previously mentioned, transitions in the $\pi h_{11/2} \otimes \nu h_{11/2}$ and the $\pi(g_{7/2}, d_{5/2}) \otimes \nu h_{11/2}$ bands were found to be of $M1/E2$ and $E2$ character. Calculations of the in-band transition strengths $B(M1{:}I \rightarrow I-1)$ and $B(E2{:}I \rightarrow I-2)$ were performed for the $\pi h_{11/2} \otimes \nu h_{11/2}$ and the $\pi g_{7/2} \otimes \nu h_{11/2}$ orbital configurations in ^{140}Eu using the particle-rotor model with triaxial deformation, $\gamma \sim 25°$. The reduced transition probability ratio is defined as

$$\frac{B(M1;I \rightarrow I-1)}{B(E2;I \rightarrow I-2)} = 0.697 \frac{1}{1+\delta^2} \frac{I_\gamma(\Delta I=1)}{I_\gamma(\Delta I=2)} \times \frac{E_\gamma^5(\Delta I=2)}{E_\gamma^3(\Delta I=1)} (\mu_N/e\ \mathrm{b})^2,$$

where E_γ is the energy in MeV of the γ ray from an initial state of spin I to a final state with spin $(I-1)$ for the $\Delta I=1$ transition or $(I-2)$ for the $\Delta I=2$ crossover transition. δ^2 is the $E2/M1$ intensity ratio for the $\Delta I=1$ transition and can be estimated from the formula [25]

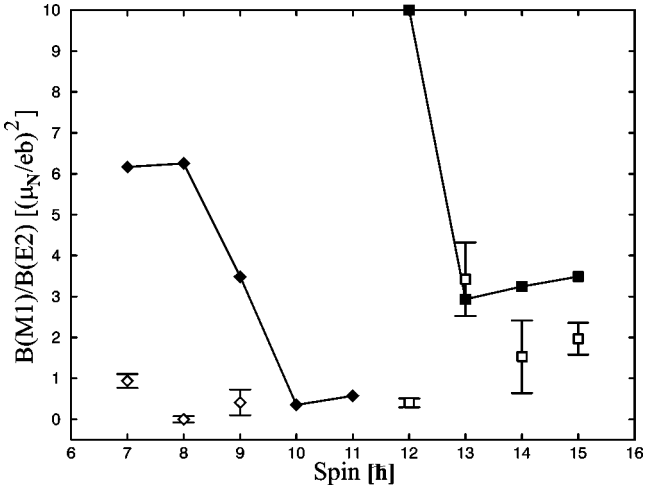

FIG. 13. Reduced transition strength ratio $B(M1)/B(E2)$ for in-band transitions. Open symbols are data while the filled symbols with solid lines are calculations. Diamonds are for band 1, squares for band 3. See text for details.

$$\frac{I_\gamma(\Delta I=1)}{I_\gamma(\Delta I=2)} = (1+\delta^{-2}) \frac{2K^2(2I-1)}{[(I+1)(I-1+K)(I-1-K)]} \times \left[\frac{E_\gamma(\Delta I=1)}{E_\gamma(\Delta I=2)}\right]^5.$$

Measured values for the reduced transition probability ratio $B(M1)/B(E2)$ are presented along with the calculated values in Fig. 13 and Table II. For band 3, there is a reasonable agreement between the measured $B(M1)/B(E2)$ values and the calculated values for spin $I=13\hbar$ and above. For band 1, on the other hand, experimental $B(M1)/B(E2)$ values are far off those of the particle-rotor model calculations, perhaps due to mixing of the positive parity proton configurations at low spins. Unfortunately, we do not have measurements of the individual $B(M1)$ or $B(E2)$ values. Lifetime measurements are needed to compare individual $B(M1)$ and $B(E2)$ values with calculations to clarify the discrepancy. In addition to in-band branching ratios, in-band to out-of-band transition branching ratios, $B(M1{:}I \rightarrow I-1)_{in}/B(M1{:}I \rightarrow I-1)_{out}$ and $B(E2{:}I \rightarrow I-2)_{in}/B(E2{:}I \rightarrow I-2)_{out}$ were measured for several transitions in bands 2 and 3. These values are also presented in Table II.

C. Possible chiral structures in ^{140}Eu

We now turn to a discussion of possible chiral band structures in ^{140}Eu. We note that chiral band partners must both have the same orbital configuration, but point out that this configuration is not limited to the $\pi h_{11/2} \otimes \nu h_{11/2}$ orbital configuration. Indeed, in ^{118}I chiral band candidates were found in the $\pi g_{9/2} \otimes \nu h_{11/2}$ bands [10] and in ^{188}Ir in the $\pi h_{11/2} \otimes \nu i_{13/2}$ bands [11]. So far, however, in the mass $A \sim 130$ region all chiral band pairs have been found to have $\pi h_{11/2} \otimes \nu h_{11/2}$ orbital configuration. In this respect, it is important that both bands 3 and 4 have a $\pi h_{11/2} \otimes \nu h_{11/2}$ configuration. Furthermore, the bands exhibit a near degeneracy of levels of

TABLE II. Comparison of experimental and calculated $B(M1)/B(E2)$ values for transitions in band 1 and in band 3. Also shown are the measured $B(E2_{out})/B(E2_{in})$ values, and the measured $B(M1_{230})/B(M1_{258})$ value for the 230 and 258 keV transitions in band 2.

Band	$I_{initial}$ $\hbar$	Experiment $\frac{B(M1_{in}:I\rightarrow I-1)}{B(E2_{in}:I\rightarrow I-2)}$ $(\mu_N/e\ \mathrm{b})^2$	Calculation $\frac{B(M1_{in}:I\rightarrow I-1)}{B(E2_{in}:I\rightarrow I-2)}$ $(\mu_N/e\ \mathrm{b})^2$
1	7	0.94(17)	6.17
1	8	0.00(08)	6.25
1	9	0.41(31)	3.49
1	10		0.35
1	11		0.57
3	12	0.40(11)	10.20
3	13	3.42(90)	2.93
3	14	1.53(89)	3.25
3	15	1.97(39)	3.49
		$\frac{B(E2_{out}:I\rightarrow I-2)}{B(E2_{in}:I\rightarrow I-2)}$	
2	12	2.66(80)	
3	15	1.05(10)	
		$\frac{B(M1_{230}:I\rightarrow I-1)}{B(M1_{258}:I\rightarrow I-1)}$	
2	13	2.20(11)	

the same spin, typical of chiral partner bands, with a difference of only ~30 keV at spins 13$\hbar$ and 15$\hbar$ to ~140 keV at spins 11$\hbar$ and 17$\hbar$. Therefore, band 4 may be the chiral partner band to band 3.

Interestingly, bands 1 and 2 are both assigned the same $\pi(g_{7/2}, d_{5/2})\otimes\nu h_{11/2}$ orbital configuration. Similar to the relation between bands 3 and 4, the levels of the same spin in bands 1 and 2 are also nearly degenerate, with a separation of ~110 keV for the 6^- and 8^- levels, and only ~10 keV for the 10^- level. Added to that, the $\Delta I=1$ band segment feeding into band 1 is similar to the $\Delta I=1$ high spin structure of band 2. This leads to the interesting possibility that perhaps bands 1 and 2 are also chiral partners. The Fermi surface is about midshell for the $g_{7/2}$ and $d_{5/2}$ orbitals and their angular momenta are less than the $h_{11/2}$ orbital. Thus the proton angular momentum vector is not predicted to be as strongly oriented toward a nuclear axis as for the $h_{11/2}$ particle and the total angular momentum vector would not be as strongly aplanar. TRS calculations predict similar deformation minima at $\gamma=25°$ for the $g_{7/2}$ or $d_{5/2}$ proton coupled with a $h_{11/2}$ neutron as for the $\pi h_{11/2}\otimes\nu h_{11/2}$ configuration, so the total deformation is predicted to be triaxial, and the total angular momentum still may be aplanar. Thus we have the interesting possibility that bands 1 and 2 may also be chiral twin partners. Of course, this is only speculative since, in contrast to the double-intruder $\pi h_{11/2}\otimes\nu h_{11/2}$ configuration, there are several natural parity proton orbitals near the Fermi surface, allowing many possibilities for a total negative parity band structure. It is always possible that an accidental degeneracy of levels in such structure occurs. To clarify the situation, further measurements are required, such as are discussed below.

However, there is a problem with the chiral interpretation. In the chiral scenario, the signature splitting within the yrast and yrare chiral bands should be small, leading to $\Delta I=1$ bands. In this context, the lack of evident signature partners for bands 4 and 2 is troublesome. It is possible that the intensity of the signature partner bands may be below the sensitivity of this experiment. A rough estimate of the population intensity range of the weaker partner for a variety of signature splittings can be obtained from an examination of several of the nuclei populated in the current experiment. For example, in ^{140}Eu, the weaker partner of band 3, the levels with odd spin, is populated with about 15–20 % the intensity of the favored signature (splitting ~100 keV). The odd neutron neighbor ^{137}Sm has a signature splitting of 100–150 keV in the $\nu h_{11/2}$ yrast band [26]. The less favored signature partner of this band is clearly identifiable in our data, with an intensity about 70% that of the favored signature. For the $\pi h_{11/2}$ yrast band of the odd proton neighbor ^{141}Eu, the splitting is 350–400 keV and the intensity of the signature partner drops to about 10% of the favored signature [27]. We point out that the typical observed splitting within a $\pi h_{11/2}\otimes\nu h_{11/2}$ chiral band in the region is about 50–100 keV, and the splitting within band 3 ~100 keV. Assuming, as a rough estimate, that the unobserved partners of band 4 and band 2 were populated with an intensity ratio of ~15–20 %, we would expect a relative intensity of transitions in bands 2 and 4 of ~5%. If this rough estimate is generous, then the signature partners of bands 4 and 2 could be easily missed. Therefore, the "missing partners" do not necessarily rule out the chiral interpretation for band 2 and band 4.

D. Shape coexistence

Another interesting possible interpretation for the bands is that of shape coexistence. Shape coexistence is well established in this mass region, some examples can be found in Ref. [3]. The examples of shape coexistence in the region are typically found for bands based on different orbital configurations polarizing the nucleus to different shapes, but even in the even-even core of ^{140}Eu (^{138}Sm), shape coexistence is suggested for two bands having the same orbital configuration [13]. In that example, for one deformation the band built on the $\pi(h_{11/2}, g_{7/2})\otimes\nu(h_{11/2})^2$ configuration shows a negligible signature splitting and the signature partner is clearly evident. For the other deformation built on the same orbital configuration, only one signature is observed. For ^{140}Eu, TRS calculations for any reasonable proton and neutron configurations predict well defined coexisting minima at $\beta\sim0.2$ and $\gamma\sim\pm25°$. These minima coexist and persist over a wide frequency range, from $\hbar\omega\sim0$ to ~0.45 MeV (see Fig. 9). Thus, if a principal axis cranking model is more applicable in the case of ^{140}Eu, it is reasonable to suggest that bands 3 and 4, while both being based on the $\pi h_{11/2}\otimes\nu h_{11/2}$ configuration, may be based on different γ deformations, and likewise for bands 1 and 2, both built on the $\pi(g_{7/2}, d_{5/2})\otimes\nu h_{11/2}$ configuration.

Once again, the lack of evident signature partner bands for bands 2 and 4 is a problem. For the $\pi h_{11/2} \otimes \nu h_{11/2}$ configuration, for β_2=0.2, β_4=−0.021, $\gamma \sim -26°$, and at a frequency of $\hbar\omega$=0.30 MeV (about midrange for the observed band and before any band crossings), the calculated signature splitting for the proton (neutron) $h_{11/2}$ orbitals is $\Delta E_p \sim 400$ keV ($\Delta E_n \sim 100$ keV). On the other hand, for the positive γ minimum with β_2=0.16, β_4=−0.021, and $\gamma \sim +28°$, we expect $\Delta E_p \sim 300$ keV ($\Delta E_n \sim 0$ keV). We note that for a doubly odd nucleus to have only one ΔI=2 band observed requires a large signature splitting for *both* the proton and the neutron orbitals. While the proton splitting is indeed estimated to be large for both deformations the neutron splitting estimate is only small or moderate, but is definitely larger for the negative γ deformation. Thus, in this scenario, band 4 may correspond to the $\pi h_{11/2} \otimes \nu h_{11/2}$ configuration based on the negative γ deformation while band 3 may correspond to the same quasiparticle configuration based on the positive γ minimum.

IV. CONCLUSION

In conclusion, we have developed the high spin level scheme for ^{140}Eu following the reaction ^{92}Mo(^{51}V, 2*pn*) at a beam energy of 205 MeV. A total of 5 bands and 69 transitions were placed in the new level scheme. The doubly intruder $\pi h_{11/2} \otimes \nu h_{11/2}$ configuration was assigned to bands 3 and 4, while the $\pi(g_{7/2}, d_{5/2}) \otimes \nu h_{11/2}$ configuration was assigned to bands 1 and 2. The interpretation for band 5 is unclear.

Both bands 1 and 2 as well as bands 3 and 4 show some of the features expected from chiral twin bands, namely, based on the same orbital configuration and having a near degeneracy of levels of the same spin and parity. However, TRS calculations indicate that there are two minima close in energy in the potential energy surface at deformations of $\beta \sim 0.2$ and $\gamma \sim \pm 25°$, allowing the possibility that these band pairs are indicative of shape coexistence. Thus we have two possible scenarios for bands 1 and 2 and bands 3 and 4. In both scenarios the lack of a second ΔI=2 sequence for the weaker partner band presents a problem. For the chiral interpretation we expect the level degeneracy between the two chiral partners to increase up to $I \sim 15\hbar$ as indeed is observed for the odd spin sequence in bands 3 and 4 and for the even spin sequence in bands 1 and 2. In addition, the chiral model predicts [28] a large jump in $B(E2)$ values for the intraband transitions around the same spin. In contrast, for shape coexistence the signature splitting should increase with rotational frequency up to the band crossing, while the corresponding $B(E2)$ values should show a smooth increase. Lifetime experiments are required to resolve this dilemma.

ACKNOWLEDGMENTS

This work was supported by the U.S. DOE under Grant Nos. DE-FG02-91ER-40609, DE-FG05-96ER-40983, and DE-FG02-88ER-40417, by the NSF under Grant No. PHY-0300673, and by the DFG under Grant No. Pi 393/1.

[1] R. F. Casten and P. von Brentano, Phys. Lett. B **152**, 22 (1985).
[2] Y. S. Chen, S. Frauendorf, and G. A. Leander, Phys. Rev. C **28**, 2437 (1983).
[3] E. S. Paul *et al.*, J. Phys. G **20**, 1405 (1994); M. A. Cardona, S. Lunardi, D. Bazzacco, G. deAngelis, and V. Roca, Phys. Rev. C **44**, 891 (1991); E. S. Paul, D. B. Fossan, Y. Liang, R. Ma, and N. Xu, *ibid.* **40**, 1255 (1989); M. Muller-Veggian, H. Beuscher, D. R. Haenni, R. M. Lieder, and A. Neskakis, Nucl. Phys. **A417**, 189 (1984).
[4] S. Frauendorf and Jie Meng, Nucl. Phys. **A617**, 131 (1997).
[5] K. Starosta *et al.*, Phys. Rev. Lett. **86**, 971 (2001); A. A. Hecht *et al.*, Phys. Rev. C **63**, 051302 (2001); T. Koike, K. Starosta, C. J. Chiara, D. B. Fossan, and D. R. LaFosse, *ibid.* **63**, 061304(R) (2001); R. A. Bark, A. M. Baxter, A. P. Byrne, G. D. Dracoulis, T. Kibédi, T. R. McGoram, and S. M. Mullins, Nucl. Phys. **A691**, 577 (2001).
[6] A. Bohr and B. R. Mottelson, *Nuclear Structure* (Benjamin, New York, 1969).
[7] D. J. Hartley *et al.*, Phys. Rev. C **64**, 031304(R) (2001).
[8] S. Frauendorf and J. Meng, Z. Phys. A **356**, 263 (1996).
[9] R. Bengtsson and S. Frauendorf, Nucl. Phys. **A314**, 27 (1979); **A327**, 139 (1979).
[10] K. Starosta, T. Koike, C. J. Chiara, D. B. Fossan, and D. R. LaFosse, Nucl. Phys. **A682**, C375 (2001).
[11] D. Balabanski *et al.*, in *International Symposium on Nuclear Structure Physics, Göttingen, Germany*, edited by R. F. Casten, J. Jolie, U. Kneissl, and K. P. Lieb (World Scientific, Singapore, 2001), p. 325.
[12] W. Nazarewicz, J. Dudek, R. Bengtsson, T. Bengtsson, and I. Ragnarsson, Nucl. Phys. **A435**, 397 (1985).
[13] E. S. Paul *et al.*, J. Phys. G **20**, 1405 (1994).
[14] R. B. Firestone, J. Gilat, J. M. Nitschke, P. A. Wilmarth, and K. S. Vierinen, Phys. Rev. C **43**, 1066 (1991).
[15] A. A. Hecht *et al.*, in *Mapping the Triangle*, edited by Ani Aprahamian, Jolie A. Cizewski, Stuart Pittel, and N. Victor Zamfir, AIP Conf. Proc. No. 638 (AIP, Melville, NY, 2002), p. 243.
[16] M. N. Tantawy *et al.*, Bull. Am. Phys. Soc. **47**, 70 (2002).
[17] D. M. Cullen *et al.*, Phys. Rev. C **66**, 034308 (2002).
[18] C. W. Beausang *et al.*, Nucl. Instrum. Methods Phys. Res. A **452**, 431 (2000).
[19] G. Duchene, F. A. Beck, P. J. Twin, G. de France, D. Curien, L. Han, C. W. Beausang, M. A. Bentley, P. J. Nolan, and J. Simpson, Nucl. Instrum. Methods Phys. Res. A **432**, 90 (1999).
[20] D. C. Radford, Nucl. Instrum. Methods Phys. Res. A **361**, 297 (1995).
[21] Y. Liu, J. Lu, Y. Ma, S. Zhou, and H. Zheng, Phys. Rev. C **54**, 719 (1996).

[22] *Table of Isotopes*, 8th ed., edited by R. B. Firestone, V. S. Shirley, C. M. Baglin, S. Y. F. Chu, and J. Zipkin (Wiley, New York, 1996).
[23] Woods-Saxon quasiparticle Routhian calculation code from http://ns.ph.liv.ac.uk/
[24] C. J. Gallagher and S. A. Moszkowski, Phys. Rev. **111**, 1282 (1958).
[25] M. A. C. Hotchkis *et al.*, Nucl. Phys. **A530**, 111 (1991).
[26] R. Ma *et al.*, Phys. Rev. C **40**, 156 (1989).
[27] N. Xu *et al.*, Phys. Rev. C **43**, 2189 (1991).
[28] Jing-ye Zhang *et al.*, in *Mapping the Triangle*, edited by Ani Aprahamian, Jolie A. Cizewski, Stuart Pittel, and N. Victor Zamfir, AIP Conf. Proc. No. 638 (AIP, Melville, NY, 2002), p. 117.